

Numerical analysis of volume loss caused by tunnel face instability in soft soils

Z. X. Zhang¹ · C. Liu² · X. Huang¹

Received: 10 March 2017 / Accepted: 7 August 2017 / Published online: 20 August 2017
© Springer-Verlag GmbH Germany 2017

Abstract This study investigates the critical support pressure at collapse on the tunnel face at different cover-to-diameter (C/D) ratios. During shallow tunnelling, the cover-to-diameter ratios may change from a positive to a negative value. The collapse of tunnel face was modelled with the use of finite element analyse (FEA) with consideration of different soil strength parameters, cover-to-diameter ratios and support pressure distribution patterns. The numerical simulations were verified against published experimental data for different C/D ratios, and the results agree well with each other. A design chart for determining the critical support pressure at collapse under undrained conditions is developed based on the FEA results. The effectiveness of the design chart in conjunction with volume loss predicted by Klar and Klein's equation to predict volume loss at collapse failure for tunnelling in soft soils is demonstrated through two case histories.

Keywords TBM · Tunnel · Face stability · FEM · Case study · Parametric study

Introduction

The shield tunnelling method can have gentle impact on surrounding environment due to its excavation efficiency and support effectiveness. Therefore, development of

underground space in recent decades prompts tunnel construction using this method, especially in congested metropolises. Furthermore, apart from normal size tunnels (usually with a diameter (D) smaller than 10 m), a number of super large tunnels have been constructed around the world, e.g. the Groene Hart Tunnel ($D = 14.87$ m) in the Netherlands and the Yangtze River Tunnel ($D = 15.43$ m) at Shanghai of China. The face stability is the most critical issue for shield tunnelling. Two types of issues can be observed during shield tunnelling when the face support pressure is not well managed: (1) collapse associated with insufficient face support pressure; and (2) blow-out owing to excessive face support pressure. The face stability of shield tunnels can be influenced by many factors including the physical and mechanical properties of the surrounding ground, the characteristics of shield machine and its operation parameters. The face stability has become a more challenging issue with increasing tunnel size as difference between support pressure and earth pressure at the tunnel crown and that at the invert can no more be neglected (Li et al. 2009).

Multiple approaches have been proposed for investigating the stability of tunnel face. Different analytical solutions have been proposed to determine the critical face support pressures within the frameworks of limit equilibrium (Horn 1961; Anagnostou and Kovari 1994; Kanayasu et al. 1995; Broere 2001; Chen et al. 2015) and limit analysis (Broms and Bennermark 1967; Davis et al. 1980; Leca and Dormieux 1990, 1992; Soubra 2000, 2002; Lee et al. 2003; Mollon et al. 2010, 2013). There have also been abundant experimental studies including those under 1-g condition (Chen et al. 2013; Fan and Zhang 2013) and centrifuge tests (Mair 1979; Chambon and Corte 1994; Kamata and Mashimo 2003; Idinger et al. 2011; Wong et al. 2012). These experiments provide researchers with

✉ Z. X. Zhang
zxzhang@tongji.edu.cn

¹ Department of Geotechnical Engineering, School of Civil Engineering, Tongji University, Shanghai 200092, China

² School of Civil Engineering, Guangzhou University, Guangzhou 510006, China

fundamental knowledge of the failure process at tunnel face. In comparison with the analytical approaches and physical experiments, numerical tools, such as finite element method (FEM), finite difference method (FDM), and discrete element method (DEM), are more efficient and economic approaches for investigating tunnel face failure. The first comprehensive FEM study on the face stability of shield tunnels was carried out by Vermeer et al. (2002), who used stepwise-reduced support pressure to achieve collapse failure at tunnel face. Besides FEM, FDM is also frequently employed in tunnel face stability analysis (Zhang et al. 2015). DEM becomes more and more popular recently for failure problems in geotechnical engineering, attributing to its inherent ability in simulating granular materials and associated large deformation (Maynar and Rodriguez 2005; Karim 2007; Zhang et al. 2011; Chen et al. 2011). However, the extremely high computational cost of DEM has limited its applications in simulating the large-scale tunnelling problems (Maynar and Rodriguez 2005). Despite the abundance of numerical studies, most of them are conducted for a special case and thus lack generality. Furthermore, there is no such study that links the support pressure with ground volume loss which is the major concern during shield tunnelling.

This study aims at evaluating tunnelling-induced volume loss during shield tunnelling based on nonlinear finite element analysis (FEA). A series of finite element (FE) models are employed considering different shear strengths of soil, different cover-to-diameter ratios, and different distribution patterns of support pressure. A comprehensive analysis on the relationships between stability state at collapse and the aforementioned three factors is carried out. Differences between results obtained from small-strain FEA and finite-strain FEA are discussed. Finally, two case studies are presented comparing numerical simulation results with field measurement data, to investigate the relationship between face support pressure and volume loss (ratio) which is widely applied for evaluating construction quality in practice. In the case histories, the volume loss (ratio) is evaluated using a recently proposed analytical equation (Klar and Klein 2014) based on the results of the parametric FEA which is able to provide a preliminary simulation on tunnelling process when experiment is not available.

Theoretical analysis on face stability of shield tunnels

Previous research revealed that failure mechanism of tunnel face varies in different soils (Schofield 1980; Kirsch 2010). As summarised by Mair and Taylor (1997), narrow chimney-shaped failure is observed in cohesionless soils.

In contrast, the face failure in cohesive soils is usually much wider than tunnel diameter, with the failure shape analogous to the mouth of a funnel. Multiple models have been proposed to calculate minimal face support pressure at collapse, taking account of different failure mechanisms in both cohesionless and cohesive soils. The proposed failure mechanisms in past decades are either based on limit equilibrium theory or limit analysis theory. The limit equilibrium models are more widely accepted in engineering practice due to its simplicity; however, the limit equilibrium approach is mathematically less rigorous than the limit analysis approach.

Limit equilibrium models

The most widely employed model within the frame work of limit equilibrium theory is the 3D wedge-silo model which was firstly introduced by Horn (1961). Based on the sliding mechanism assumed by Horn's model (Horn 1961), Anagnostou and Kovari (1994) investigated the face stability during the process of slurry-shield tunnelling. A series of elaborated models were proposed on the basis of the failure mechanism assumed in Horn's model (Horn 1961), considering the effect of soil-arching above tunnel crown (Anagnostou 2012; Chen et al. 2015; Jancsecz and Steiner 1994), the effect of groundwater seepage at tunnel face (Anagnostou and Kovari 1996), and the effect of soil stratification (Belter et al. 1999; Broere 2001). These approaches can be employed in evaluating the critical support pressure of tunnel face for suitable soils, making the wedge-silo model widely accepted in both academia and practice.

Limit analysis models

Based on the limit theorem of plasticity, soils are treated as an elastic, perfectly plastic material in limit analysis models. Two theorems are involved in the limit analysis, i.e. the lower bound theorem and the upper bound theorem (Chen 1975; Drucker and Prager 1952). The lower bound theorem states that the loads are lower than (or equal to) those for collapse, if any stress field can be found to support the loads and everywhere is in equilibrium without yielding (Chen 1975; Davis et al. 1980). The upper bound theorem states that the loads are higher than (or equal to) those for collapse, if the loads are deduced from the work calculation for a kinematically admissible collapse mechanism (Chen 1975; Davis et al. 1980).

Multiple failure mechanisms have also been proposed within the framework of limit analysis. According to the centrifuge tests carried out by Cairncross (1973), Mair (1979) and Davis et al. (1980) proposed four different failure mechanisms at tunnel face in pure clay, for the sake

of subsequent limit analyses of the critical face support pressures at both collapse and blow-out. Thereafter, a series of rigid block failure mechanisms have been developed in the framework of the kinematical approach in limit analysis (Mollon et al. 2013), considering different shapes of the failure block (Leca and Dormieux 1990, 1992; Soubra 2000), the effect of seepage force at the tunnel face (Lee et al. 2003), and stratification of the ground (Tang et al. 2014).

Load factor and volume loss

The load factor LF , defined as N/N_c where N and N_c are stability ratios, respectively, at current state and that at collapse failure, is commonly used to evaluate the face stability during tunnelling in clays (Mair et al. 1981; Dimmock and Mair 2007). As initially proposed by Broms and Bennermark, the stability ratio N can be defined as:

$$N = \frac{\sigma_s + \gamma z - \sigma_t}{s_u} \tag{1}$$

where γ is soil unit weight, z is cover depth to tunnel axis level, σ_s is surcharge on the ground surface, σ_t is support pressure at tunnel face, and s_u is undrained soil shear strength at the tunnel axis level. The critical stability ratio N_c can be obtained by small-scale model tests under 1-g conditions or in a centrifuge. Previous research reveals that certain relationship exists between LF and volume loss during tunnelling (Macklin 1999).

Based on the continuous velocity fields at collapse, Klar and Klein (2014) proposed that the relationship between LF and volume loss (V_L) for Tresca-type yielding soils can be expressed as:

$$\frac{V_L}{\varepsilon_{50}} = 1.85 \frac{LF}{1 - LF} \left(\frac{C}{D}\right)^{LF^{0.72}} \tag{2}$$

where C is tunnel roof cover depth and ε_{50} is the axial strain at which 50% of soil strength is mobilised.

FEA for tunnel face stability

FEA model description

In this study, a series of three-dimensional FE models are constructed based on the commercial FEA software ABAQUS (Dassault Systèmes Simulia Corp 2014). The meshes, as well as the dimensions of the numerical models, are illustrated in Fig. 1. The types and numbers of elements and nodes are also listed in this figure. In some cases, non-positive cover-to-diameter ratio may be encountered, e.g. in the Ultra Rapid Underpass (URUP) tunnelling process

(Zhang et al. 2016), during which the face stability will be more difficult to control. Therefore, six different cover depths are considered in the FEA ranging from negative cover-to-diameter ratio case to deeply buried case, i.e.

$$C/D = -0.3, 0, 0.5, 1.0, 1.5, \text{ and } 2.0$$

(as shown in Fig. 1). It is noteworthy that for the case of $C/D = 0$, wedge elements are employed for the soil adjacent to the ground surface, owing to the difficulty of structured meshing in sharp corner of the geometry (yellow coloured region in Fig. 1). According to previous research, the ‘element death’ technique is commonly employed for simulation of tunnel excavation in FEA. However, this study focuses on the relationship between the support pressure and the face stability, while the detail excavation process is not the concern of the current study. Therefore, the detail excavation process is not simulated and the soil elements within the excavation region are not created, rather the nodes in the periphery of excavated region (31 m in length) are fixed (purple faces as shown in Fig. 1). For the sake of reducing computational cost, the models considered are supposed to be symmetric in geometry. The excavation diameter (i.e. shield diameter) is 15.43 m, which is in accordance with multiple large tunnels constructed in China (Huang 2008; Liu et al. 2014). Previous researchers have shown that different support pressure distribution patterns probably result in different failure mechanisms. Therefore, as depicted in Fig. 1, both uniform and linear distributions of support pressure are taken into consideration in these models. The former indicates a support medium of compressed air in front of the tunnel face, while the latter represents the support medium of earth paste or bentonite slurry. For the uniform distribution, the maximum (or initial) pressure magnitude is expressed as

$$\sigma_T = \sigma_{T0} = K_0 \gamma (C + D/2) \tag{3}$$

where σ_T is the support pressure at tunnel face, σ_{T0} is the support pressure at tunnel centre level, K_0 is the coefficient of the lateral earth pressure at rest, γ is soil unit weight, C is the cover depth of tunnel crown, and D denotes the excavation diameter. For the linear distribution, the support pressure can be calculated as

$$\sigma_T = \sigma_{T0} + \gamma_s (z_0 - z) \tag{4}$$

where z_0 and z are, respectively, the cover depth of the tunnel centre level and the cover depth at the position of evaluation, γ_s is the unit weight of the support medium. For models with linearly distributed support pressure, σ_{T0} is reduced stepwise (0.02 σ_{T0} per calculation step) until collapse takes place which is characterised by the non-convergence in the FEA calculation.

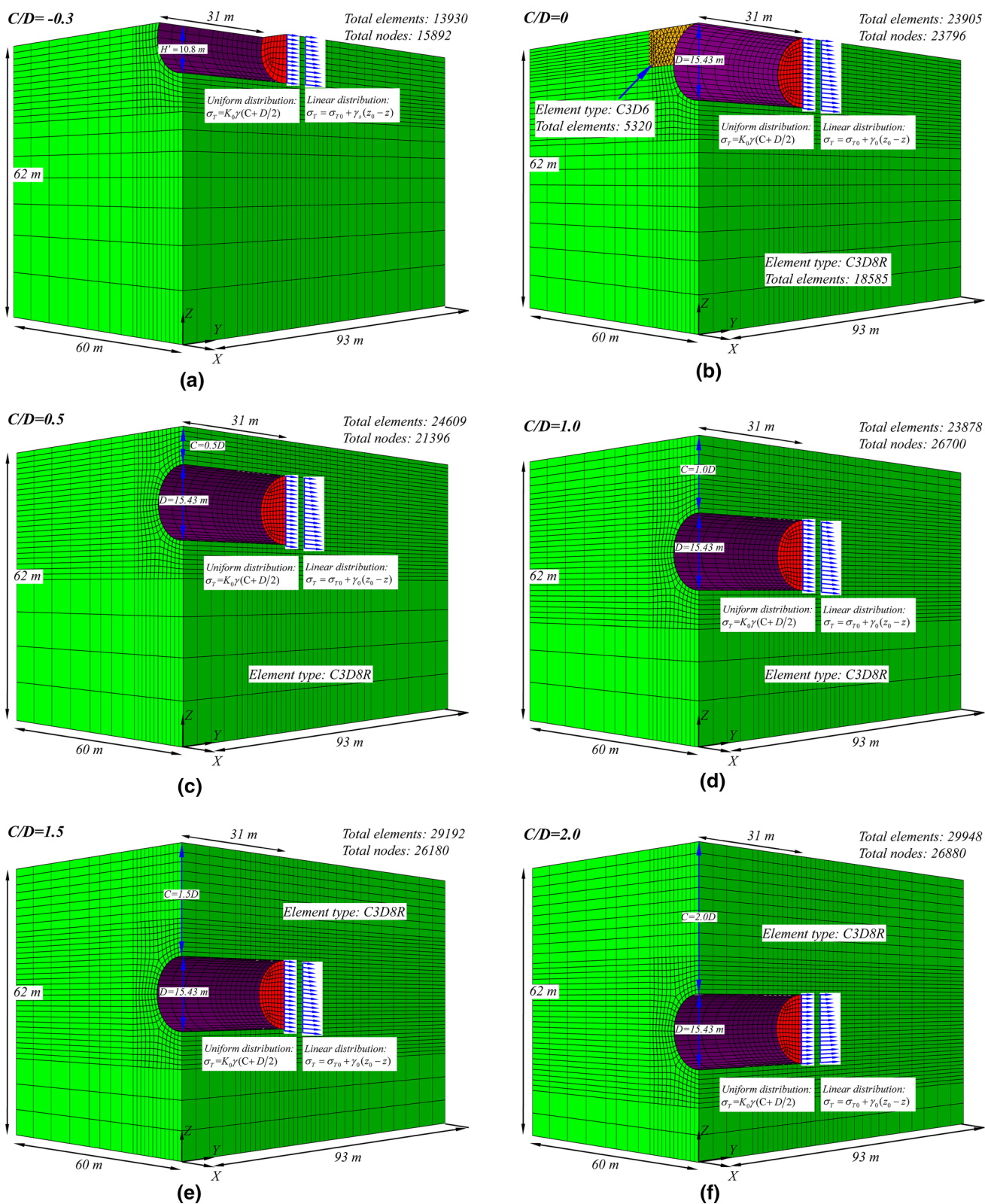


Fig. 1 Overview of the FEA models employed in the study: **a** $C/D = -0.3$; **b** $C/D = 0$; **c** $C/D = 0.5$; **d** $C/D = 1.0$; **e** $C/D = 1.5$; **f** $C/D = 2.0$

Materials and constitutive model

Soil considered in the FEA is assumed to behave as an elastoplastic material with the combination of linear elasticity and Mohr–Coulomb (MC) yield criterion. The MC yield criterion is widely adopted in geotechnical practice, ascribing to its simplicity and accuracy. The cohesion c and internal friction angle ϕ are the two most important factors for evaluating soil strength Coulomb (1773). Sandy soils are commonly characterised by negligible cohesion but considerably large friction angle, while the strength of clayey soils is determined by their inherent cohesion. Comparing with other yield criteria, the MC yield criterion can reduce the number of strength parameters while performing parametric study. Another important reason of employing this yield criterion is that the two strength parameters (i.e. cohesion and internal friction angle) are widely accepted and easily obtained in practice. In order to investigate the influence of soil properties on tunnel face stability, various combinations of c and ϕ are considered in the FEA (as listed in Table 1), while the soil unit weight, the dilation angle, and the Young’s modulus are fixed at 17 kN/m³, 0.1°, and 5 MPa, respectively. Existing research revealed that the dilation angle has little influence on the critical support pressure at collapse (Vermeer et al. 2002). Therefore, non-dilatative material is employed in this study. These parameters are supposed to be constant, allowing a direct comparison between the influence of c and that of ϕ . Coefficient of lateral earth pressure at rest (K_0) can be evaluated via

$$K_0 = 1 - \sin \phi' \tag{5}$$

where ϕ' is the effective friction angle of the soil. The Poisson’s ratio (ν) can be estimated via K_0 and determined through laboratory tests.

In nature, cohesion and friction angle of different soils (from clay to sand) are different. Even for the same soil, the two strength parameters vary with the drainage condition of the soil. Thus, different combination of the cohesion and the friction angle can be encountered in practice. In order to investigate the face stability under different soil strength parameters, the cohesion and the friction angle vary independently in the numerical simulation herein. In order to reduce computational cost, the cohesion and friction angle vary at interval values of 10 kPa and 10°, respectively. In total, 288 different cases (six cover-to-depth ratios × two support pressure distribution patterns × 24 combinations of c and ϕ) are taken into consideration in this parametric FEA, as listed in Table 1.

Small-strain analysis versus finite-strain analysis

Small-strain FEA ignores geometric nonlinearity in element calculations. The elements in a small-displacement

analysis are formulated in the reference configuration, using original nodal coordinates (Dassault Systèmes Simulia Corp 2014). For finite-strain analysis, large-displacement effects are taken into consideration in element calculations. In this case, elements are formulated in current configuration using current nodal positions (Dassault Systèmes Simulia Corp 2014). The small-strain FEA is characterised by its high computational efficiency, while the finite-strain FEA can provide accurate predictions on large deformation behaviour.

Currently, development of the TBM technology reduces significantly tunnelling-induced influence on surrounding ground. Therefore, for regular tunnelling simulations in which the ground deformation is small, FEA at small strain is enough for obtaining acceptable results. However, since this study focuses on critical support pressure at collapse failure, large deformation at the tunnel face cannot be avoided during the FEA. Taking that on board, the large-displacement formulation should be necessarily involved in the FEA. In order to investigate the difference between the calculated critical support pressure at small-strain level and that at finite-strain level, the case with $c = 10$ kPa, $\phi = 20^\circ$, and $C/D = 1.0$ is employed as a benchmark. The soil with $c = 10$ kPa and $\phi = 20^\circ$ is encountered in silty clay of several projects in China (e.g. the Qiantang River Tunnel), and the tunnel with $C/D = 1.0$ is relatively common in shallow buried condition.

A support pressure ratio (SPR) is defined with the following expression

$$SPR = \sigma_T / \sigma_v \tag{6}$$

where σ_v is the gravitational stress of the soils at the tunnel face centre, i.e. $\sigma_v = \gamma(C + D/2)$. As shown in Fig. 2a, the calculated displacement at tunnel face centre is normalised by tunnel diameter. A parameter Δu is defined in Eq. 7 to quantify the difference between displacements obtained from small-strain and finite-strain analyses, respectively,

$$\Delta u = u_{\text{small}} - u_{\text{finite}} \tag{7}$$

where u_{small} and u_{finite} are calculated u in small-strain FEA and finite-strain FEA, respectively. Similarly, Δu is also normalised by tunnel diameter D , and plotted against SPR in Fig. 2b.

As shown in Fig. 2a, a typical dramatic increase in normalised displacement can be observed when $SPR < 0.09$. According to previous research of FEA on tunnel face stability (Vermeer et al. 2002; Lu et al. 2014), the collapse occurs when the pressure–displacement curve becomes horizontal. However, as illustrated in Fig. 2a, SPR did not strictly approach a constant value when the soil has the trend to flow, indicating that the critical support pressure in this study was slightly greater than that obtained during transition from solid to liquid state in soils at tunnel face. In spite of this, these values are

Table 1 c and ϕ for the soils in the FEA

	$\phi = 0.3^\circ$	$\phi = 10^\circ$	$\phi = 20^\circ$	$\phi = 30^\circ$	$\phi = 40^\circ$
$c = 0.01$ kPa		$\gamma = 17$ kN/m ³ $K_0 = 0.83$ $\nu = 0.45$ $\psi = 0.1^\circ$ $E = 5$ MPa	$\gamma = 17$ kN/m ³ $K_0 = 0.66$ $\nu = 0.40$ $\psi = 0.1^\circ$ $E = 5$ MPa	$\gamma = 17$ kN/m ³ $K_0 = 0.5$ $\nu = 0.33$ $\psi = 0.1^\circ$ $E = 5$ MPa	$\gamma = 17$ kN/m ³ $K_0 = 0.36$ $\nu = 0.26$ $\psi = 0.1^\circ$ $E = 5$ MPa
$c = 10$ kPa	$\gamma = 17$ kN/m ³ $K_0 = 1$ $\nu = 0.48$ $\psi = 0.1^\circ$ $E = 5$ MPa	$\gamma = 17$ kN/m ³ $K_0 = 0.83$ $\nu = 0.45$ $\psi = 0.1^\circ$ $E = 5$ MPa	$\gamma = 17$ kN/m ³ $K_0 = 0.66$ $\nu = 0.40$ $\psi = 0.1^\circ$ $E = 5$ MPa	$\gamma = 17$ kN/m ³ $K_0 = 0.5$ $\nu = 0.33$ $\psi = 0.1^\circ$ $E = 5$ MPa	$\gamma = 17$ kN/m ³ $K_0 = 0.36$ $\nu = 0.26$ $\psi = 0.1^\circ$ $E = 5$ MPa
$c = 20$ kPa	$\gamma = 17$ kN/m ³ $K_0 = 1$ $\nu = 0.48$ $\psi = 0.1^\circ$ $E = 5$ MPa	$\gamma = 17$ kN/m ³ $K_0 = 0.83$ $\nu = 0.45$ $\psi = 0.1^\circ$ $E = 5$ MPa	$\gamma = 17$ kN/m ³ $K_0 = 0.66$ $\nu = 0.40$ $\psi = 0.1^\circ$ $E = 5$ MPa	$\gamma = 17$ kN/m ³ $K_0 = 0.5$ $\nu = 0.33$ $\psi = 0.1^\circ$ $E = 5$ MPa	$\gamma = 17$ kN/m ³ $K_0 = 0.36$ $\nu = 0.26$ $\psi = 0.1^\circ$ $E = 5$ MPa
$c = 30$ kPa	$\gamma = 17$ kN/m ³ $K_0 = 1$ $\nu = 0.48$ $\psi = 0.1^\circ$ $E = 5$ MPa	$\gamma = 17$ kN/m ³ $K_0 = 0.83$ $\nu = 0.45$ $\psi = 0.1^\circ$ $E = 5$ MPa	$\gamma = 17$ kN/m ³ $K_0 = 0.66$ $\nu = 0.40$ $\psi = 0.1^\circ$ $E = 5$ MPa	$\gamma = 17$ kN/m ³ $K_0 = 0.5$ $\nu = 0.33$ $\psi = 0.1^\circ$ $E = 5$ MPa	$\gamma = 17$ kN/m ³ $K_0 = 0.36$ $\nu = 0.26$ $\psi = 0.1^\circ$ $E = 5$ MPa
$c = 40$ kPa	$\gamma = 17$ kN/m ³ $K_0 = 1$ $\nu = 0.48$ $\psi = 0.1^\circ$ $E = 5$ MPa	$\gamma = 17$ kN/m ³ $K_0 = 0.83$ $\nu = 0.45$ $\psi = 0.1^\circ$ $E = 5$ MPa	$\gamma = 17$ kN/m ³ $K_0 = 0.66$ $\nu = 0.40$ $\psi = 0.1^\circ$ $E = 5$ MPa	$\gamma = 17$ kN/m ³ $K_0 = 0.5$ $\nu = 0.33$ $\psi = 0.1^\circ$ $E = 5$ MPa	$\gamma = 17$ kN/m ³ $K_0 = 0.36$ $\nu = 0.26$ $\psi = 0.1^\circ$ $E = 5$ MPa

chosen as corresponding critical support pressures at collapse for the sake of safety. As shown in Fig. 2b, difference between $\Delta u/D$, respectively, at small strain and finite strain becomes evident while SPR is less than 0.1, indicating that FEA at small strain probably underestimates the critical support pressure at collapse failure. In addition, comparing with the finite-strain analysis, the small-strain analysis is not able to include the large-displacement effects, that is the elements cannot be used after they are severely distorted (e.g. negative element volume at an integration point) due to sufficiently large deformations. Thus, the finite-strain FEA is adopted in the parametric study.

FEA results and discussions

Influence of c and ϕ on SPR

Relationship among soil cohesion (c), soil friction angle (ϕ), cover-to-diameter ratio (C/D), and SPR is illustrated in Fig. 3. Both the results for uniform and linear distribution patterns of the support pressure are presented in the

figure. The line intersections in the illustrated contours represent results obtained in the FEA at finite strain. The contour values are calculated by spline interpolation. A higher critical SPR implies that the face stability is more difficult to maintain. Generally, SPR decreases with increasing c and ϕ in all cases with the selected cover-to-diameter ratios in this study. This is in accordance with the numerical study of Lu et al. (2014) in which the critical support pressure decreased with increasing frictional angle (the cohesion was fixed at 2 kPa). By comparison between the results obtained via uniformly and linearly distributed support pressure, it can be observed that the uniformly distributed support pressure seems to result in a higher critical SPR, probably owing to the more significant shear strain ahead of the tunnel face when the uniformly distributed support pressure is applied. Previous research reveals that the pressure gradient can notably improve the local stability of the tunnel face (Li et al. 2009). As illustrated in Fig. 3a, b, which, respectively, represent cover-to-diameter ratios of -0.3 and 0 , c has more significant influence on critical SPR comparing to ϕ . In particular, for

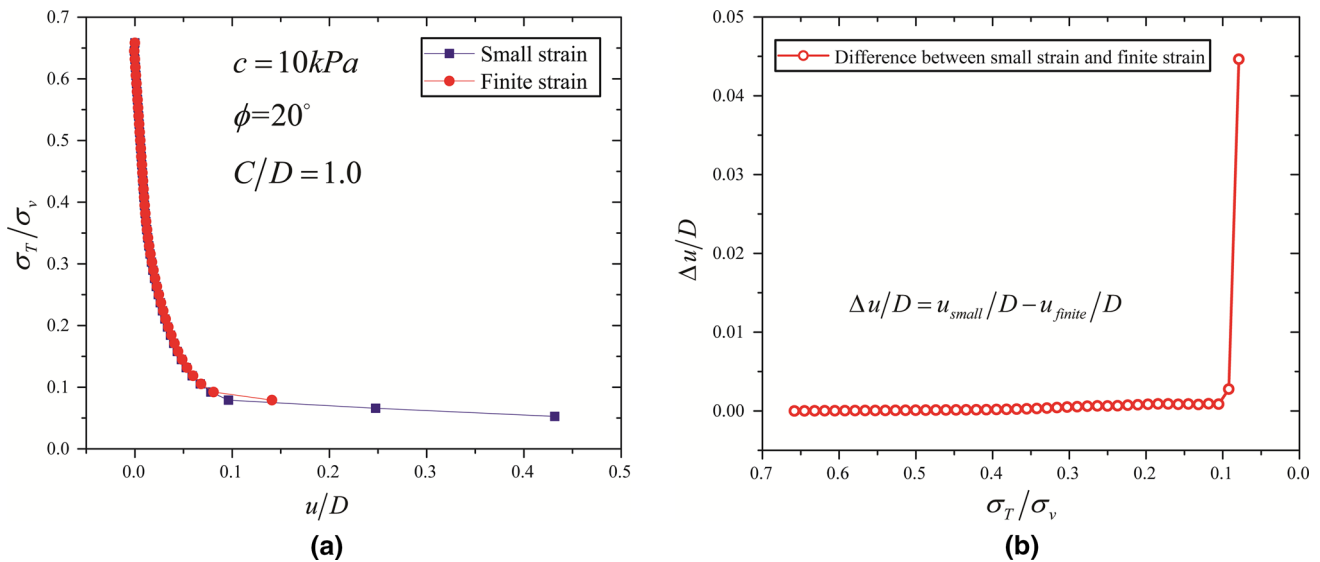


Fig. 2 Comparison between the simulation results at small strain and finite strain: **a** relationship between the SPR and the u/D ; and **b** relationship between the SPR and the $\Delta u/D$

the case with $C/D = 0$, ϕ has little influence on the interpolated critical SPR when $\phi > 10^\circ$, showing a notable difference with $\phi < 10^\circ$ under which c and ϕ are at the same level of influence on the critical SPR. By comparison among Fig. 3c–f, it can be observed that the contour inclination increases with cover-to-depth ratios, implying that the critical SPR becomes more sensitive to ϕ with increasing cover-to-depth ratio when $C/D > 0$. For the two different distributions of the support pressure, by comparison of the region within which the critical SPR is less than 0.02, it can be observed that soils with relatively high levels of c and ϕ (i.e. high shear strength) are not sensitive to the pressure distribution pattern, while the opposite phenomena can be found in soils with low shear strength.

Influence of C/D on critical support pressure (cohesionless soil)

Sandy soil in which cohesion is absent is usually selected as a typical condition for investigating failure mechanism of tunnel face at collapse. Figure 4 illustrates relationship between normalised critical support pressure and cover-to-diameter ratio (C/D). The normalised critical support pressure is defined as $\sigma_c/\gamma D$, where σ_c denotes the critical support pressure, i.e. the support pressure (σ_T) at collapse (Li 2007). A series of 1-g large-scale model tests were carried out by Chen et al. (2013). Medium grained sand collected from the Yangtze River was employed in this experiment. Laboratory tests revealed that the friction angle of the sand was 37° . The experimental data of Chen et al. are overlaid in Fig. 4 for comparison. As can be

observed from the FEA results, $\sigma_c/\gamma D$ does not experience evident variation with C/D while $\phi > 20^\circ$ and $C/D > 0$. This is in accordance with the existing experiments (Chen et al. 2013; Kirsch 2010) and theoretical prediction (Leca and Dormieux 1990). As illustrated in Leca and Dormieux (1990), the weighting coefficient N_γ at collapse equals to $\sigma_c/\gamma D$ for the tunnel in cohesionless soil without surface load. Based on the theoretical prediction of N_γ in Leca and Dormieux (1990), the calculated $\sigma_c/\gamma D$ in this study shows agreement with that predicted by the upper bound solution, that is the values of $\sigma_c/\gamma D$ under $\phi = 20^\circ, 30^\circ$, and 40° are, respectively, around 0.20, 0.11, and 0.06. It should be noted that the values of $\sigma_c/\gamma D$ of this numerical study are slightly lower than those of the upper bound solution while $\phi = 30^\circ$ and 40° . This is probably caused by the simplified failure mechanism assumed in Leca and Dormieux (1990). For natural sand encountered in geotechnical activities, the frictional angle is usually greater than 30° . Therefore, it can be concluded that cover-to-diameter ratio has limited influence on normalised critical support pressure in cohesionless soils while $C/D \leq 2.0$. According to the FEA results, soil with a friction angle less than 10° owns different relationship between $\sigma_c/\gamma D$ and C/D , i.e. the normalised critical support pressure increases consistently with C/D (see Fig. 4). This is probably caused by the low soil strength which makes the soil deform significantly. Based on the numerical data, it can be observed that the critical support pressure under certain cover-to-diameter ratio increases with decreasing friction angle, indicating that sandy soil with high shear strength is more stable than that with a low friction angle.

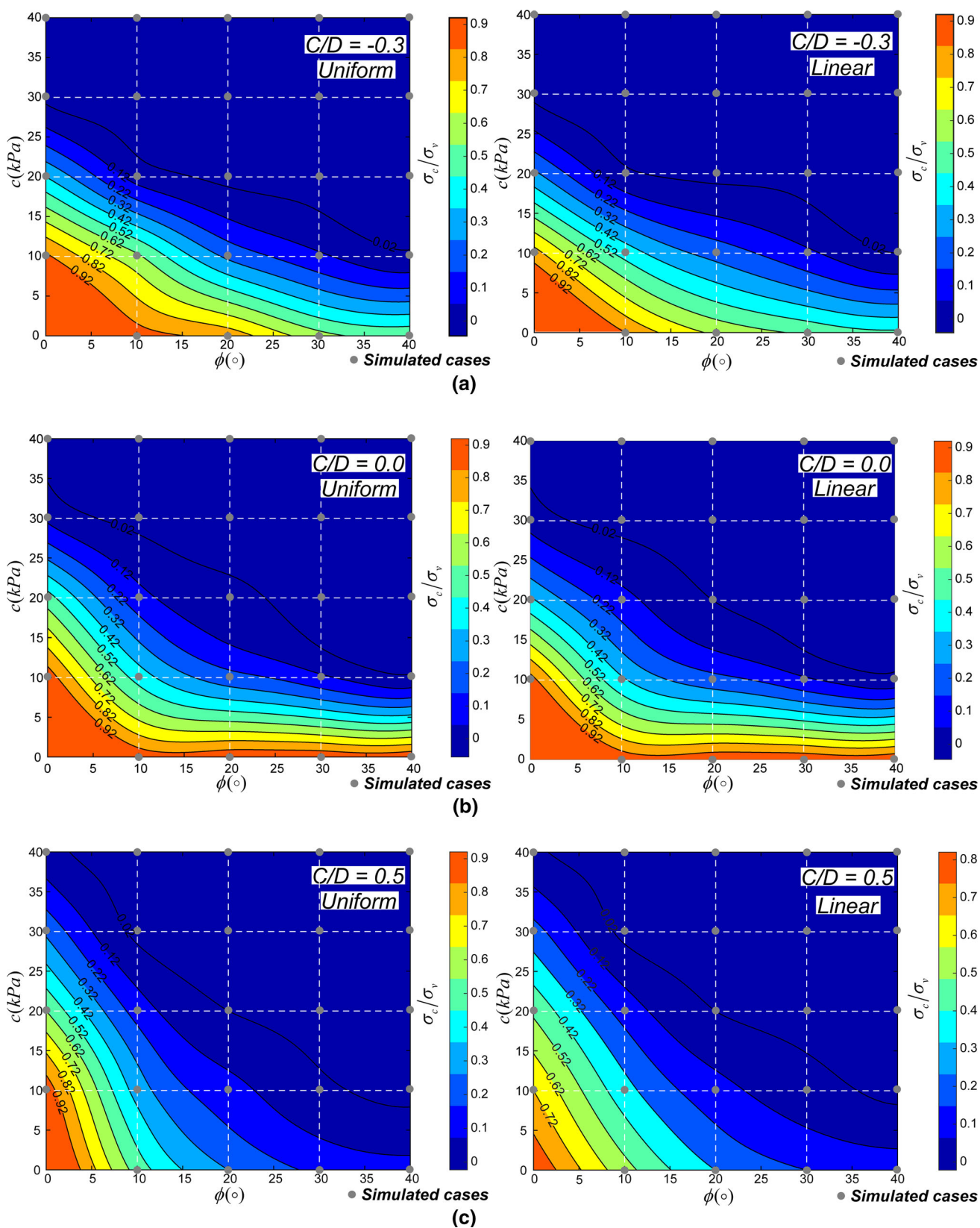


Fig. 3 Critical SPR contour under different c and ϕ : **a** $C/D = -0.3$; **b** $C/D = 0$; **c** $C/D = 0.5$; **d** $C/D = 1.0$; **e** $C/D = 1.5$; **f** $C/D = 2.0$

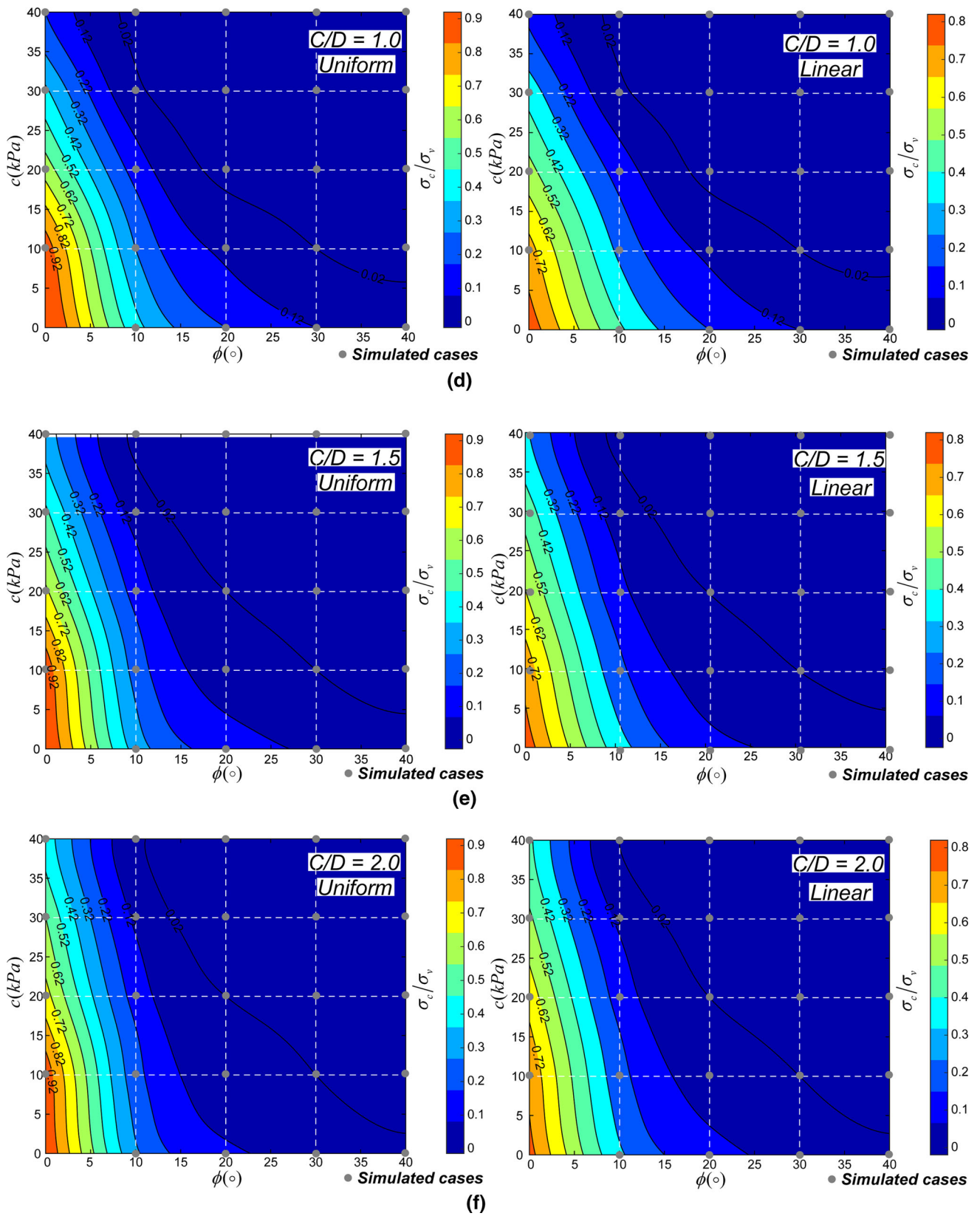


Fig. 3 continued

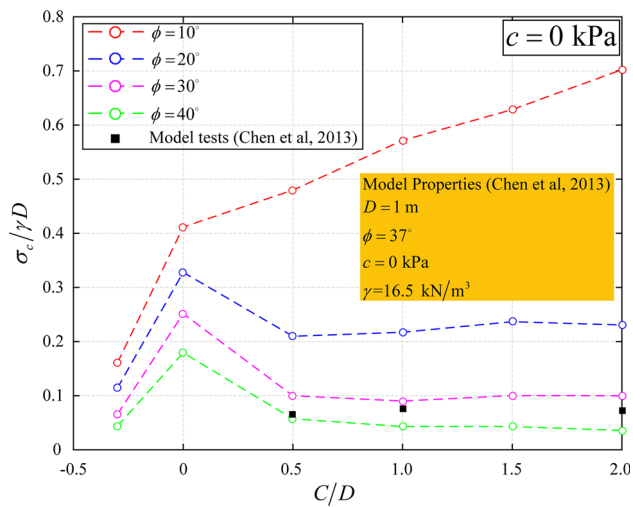


Fig. 4 Relationship between the normalised critical support pressure ($\sigma_c/\gamma D$) and the cover-to-diameter ratio (C/D) in cohesionless soil

For the cases with $C/D = 0$, it is noteworthy that the critical support pressures are obviously higher than those under other cover-to-depth ratios. Based on Fig. 3b, no evident variation in critical support pressure can be observed with increasing friction angle while the cohesion is nearly absent. This is probably attributed to the different failure modes of the tunnel face under this cover-to-depth ratio. Under this cover-to-diameter ratio, cohesionless soils will experience a significant strain development at the tunnel crown where the geometry contains sharp corners (refer to Fig. 1), making the calculation terminated at a limit support pressure that is obviously higher than other cases in which the failure points are located far away from the crown/invert at the tunnel face. This phenomenon is intuitional and also observed during tunnelling activity using the URUP (Ultra Rapid Under Pass) method. Comparing to the cases with non-negative cover-to-diameter ratios, the critical support pressure under a cover-to-diameter ratio of -0.3 shows less obvious variation with different friction angles. Based on our URUP tunnelling practice with a tunnel diameter of 6.38 m, an empty excavation chamber was observed during shield advance under negative overburden, indicating that the tunnel face did not need a high level of support pressure.

By comparison between the experiment results (Chen et al. 2013) and FEA cases of $\phi > 30^\circ$ and 40° (see Fig. 4), it can be concluded that the numerical results herein are reliable for investigating the critical support pressure in natural sand.

Influence of C/D on the stability ratio

For clayey soil under undrained condition, the friction angle can be neglected and the shear strength $s_u = c$.

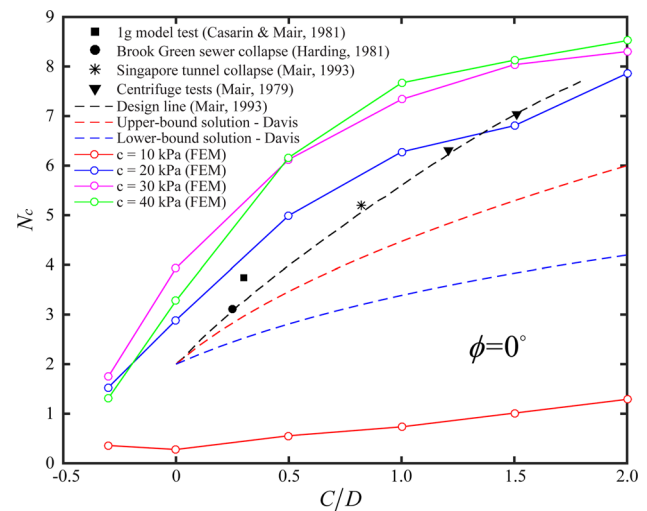


Fig. 5 Relationship between critical stability ratio and cover-to-diameter ratio in clayey soil under uniform support pressure

Figure 5 illustrates the relationship between critical stability ratio (N_c) and cover-to-diameter ratio (C/D) in pure clay under uniform support pressure. The data from a small-scale experiment (Casarin and Mair 1981), a centrifuge experiment (Mair 1979), two case histories (Harding 1981; Mair 1993), and theoretical prediction (Davis et al. 1980) are collected and plotted as references in Fig. 5. As shown in Fig. 5, N_c obtained from FEA is greater than both of the lower and upper bound solutions of Davis's theory. Since the experiments and case records herein also provide N_c greater than Davis's solutions, it can be inferred that Davis's upper bound solution does not agree well with the reality. This is probably owing to the inherent two-block assumption employed in this theoretical solution. Based on the comparison illustrated in Fig. 5, FEA with a $c = 20$ kPa provides N_c that is closer to the selected experiment and case studies. For certain cohesion (except $c = 10$ kPa), critical stability ratio has a positive correlation with cover-to-diameter ratio. This relationship also exists between soil cohesion and critical stability ratio while $C/D \geq 1.0$. With respect to the case with $c = 10$ kPa, it can be observed that critical stability ratios are evidently smaller than those with other three cohesions (refer to Fig. 5). As revealed by previous research on tunnel face stability during large shield tunnelling (Li 2008), local failure with a hemisphere mode may occur while $\gamma D/c_u \geq 10.7$. According to the FEA herein, local failure occurs in the case with $c = 10$ kPa (as shown in Fig. 6), making the critical support pressure close to γD , and hence the significantly low value of N_c .

The FEA results of the tunnel face at collapse are summarised (cohesive soils only) in Tables 2 and 3 (only the cases with linear support pressure are presented). It

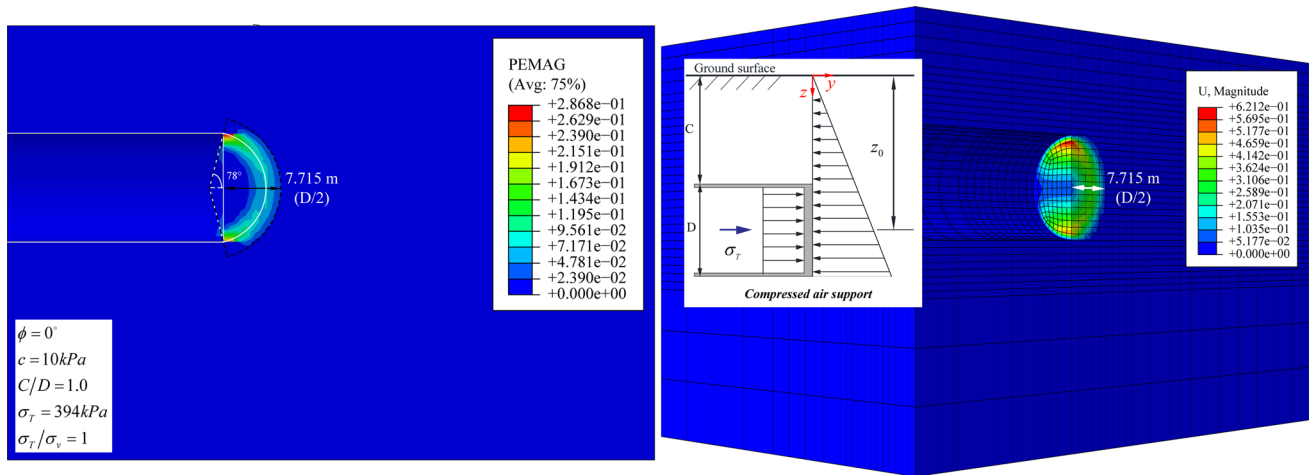


Fig. 6 Illustration of the face failure with $c = 10$ kPa, $\phi = 0^\circ$ under uniform support pressure

Table 2 FEA results for tunnel face at collapse with uniform support pressure distribution ($\phi = 0^\circ$)

s_u (kPa)	$C/D = -0.3$		$C/D = 0$		$C/D = 0.5$		$C/D = 1.0$		$C/D = 1.5$		$C/D = 2.0$	
	σ_c (kPa)	N_c	σ_c (kPa)	N_c	σ_c (kPa)	N_c	σ_c (kPa)	N_c	σ_c (kPa)	N_c	σ_c (kPa)	N_c
10	48.9	0.4	128.4	0.3	256.8	0.6	386.1	0.7	514.5	1.0	642.9	1.3
20	21.8	1.5	73.4	2.9	162.4	5.0	267.9	6.3	388.5	6.8	498.6	7.9
30	0.0	1.7	13.1	3.9	78.6	6.1	173.4	7.3	283.5	8.0	406.7	8.3
40	0.0	1.3	0.0	3.3	15.7	6.2	86.7	7.7	199.5	8.1	314.9	8.5

Table 3 FEA results for tunnel face at collapse with linear support pressure distribution ($\phi = 0^\circ$)

s_u (kPa)	$C/D = -0.3$		$C/D = 0$		$C/D = 0.5$		$C/D = 1.0$		$C/D = 1.5$		$C/D = 2.0$	
	σ_c (kPa)	N_c	σ_c (kPa)	N_c	σ_c (kPa)	N_c	σ_c (kPa)	N_c	σ_c (kPa)	N_c	σ_c (kPa)	N_c
10	44.7	0.8	125.8	0.5	188.6	7.4	299.4	9.4	409.5	11.5	524.8	13.1
20	17.7	1.7	57.6	3.7	131.0	6.6	220.6	8.6	325.5	10.0	446.1	10.5
30	0.0	1.7	10.5	4.0	68.1	6.5	149.7	8.1	252.0	9.1	354.2	10.1
40	0.0	1.3	0.0	3.3	10.5	6.3	78.8	7.9	178.5	8.7	288.6	9.2

should be noted that the critical support pressure σ_c is obtained directly from the FEA, and the undrained shear strength s_u is calculated according to the Mohr's theory:

$$s_u = (\sigma_1 - \sigma_3)/2 \quad (8)$$

where σ_1 and σ_2 are the major and minor principal stresses at tunnel face centre, respectively. The undrained shear strength commonly equals to the cohesion c_u obtained from unconsolidated undrained (UU) triaxial compression test.

Case studies

Given that the soil strength parameters and depth-to-diameter ratio of the tunnel are known, the critical stability ratio N_c can be readily obtained from Tables 2 or 3 by

interpolation and extrapolation. The volume loss can then be roughly estimated using Eq. 2. To demonstrate the applicability of this methodology, two case histories are investigated.

Face stability analysis for the Qiantang River Tunnel

FEA in this study is based on the tunnel with a diameter of 15.43 m which is in accordance with three operating tunnel projects in Yangtze River Delta of China: the Shanghai Yangtze River Tunnel, the West Changjiang Rd. Tunnel, and the Qiantang River Tunnel. Among these tunnels, the Qiantang River Tunnel is selected as a representative case for utilising the FEA results in this study.

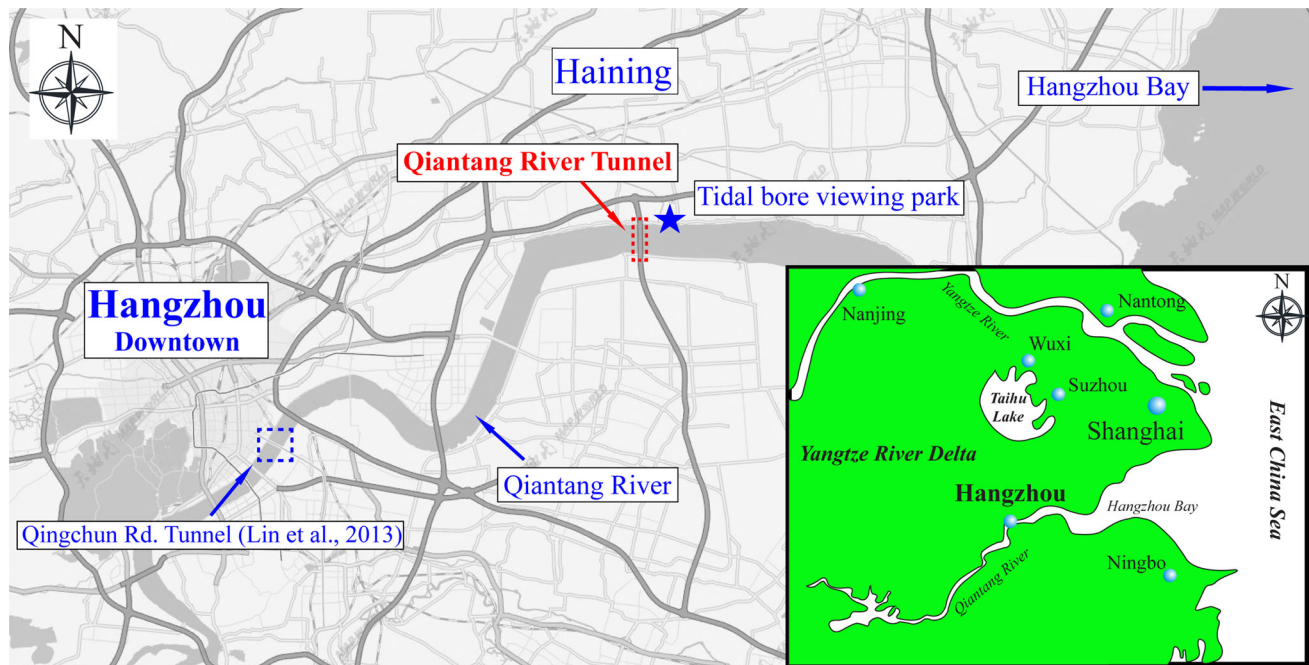


Fig. 7 Overview of the Qiantang River Tunnel

The Qiantang River Tunnel was constructed beneath the Qiantang River which runs across Hangzhou, the capital city of Zhejiang Province in East China (see Fig. 7). As illustrated in Fig. 7, the tunnel is adjacent to the tidal-bore viewing park of Haining which is a very famous scenic spot in China. A slurry-shield machine ($D = 15.43$ m) manufactured by the Herrenknecht was employed for the twin-tunnel construction. The shield machine was initially launched at the south bank of the Qiantang River and driven to the north bank along the west-bound route; the shield machine was then turned around and advanced along the east-bound (EB) route. This study focuses on ground surface settlements occurring at the south and north banks during the west-bound (WB) tunnelling which satisfies the ‘green’ field condition. The compositions of soil strata along the WB route are generally ranged from sandy silt to silty clay. An undrained condition is considered. Three sections, two of which are located at the south bank and one at the north bank, were selected for field measurements. Figure 8 illustrates soil profiles of the three selected monitoring sections along the WB tunnelling. Layouts of the surface settlement points (SSPs) on the north and south banks are shown in Fig. 9. According to previous studies, the ground volume loss induced by mechanised tunnelling activities can be generally divided into components associated with face ‘take’ and with radial ‘take’, where the former is induced by tunnel-heading soil behaviour and the latter results from overcut-induced soil convergence deformation and lining installation. Only the face ‘take’ volume loss is considered in this study.

As shown in Fig. 8a, soils in the vicinity of the launching shaft on the south bank are generally sandy silt and silt above the tunnel centre level, while clays at silty and mucky silty states are present adjacent to the receiving shaft on the other side of the river. Figure 10 shows the measured surface settlements at the SSPs with corresponding linear fits for volume loss calculation. It should be clarified that the SSPs WR28 W-3 and WR1610 W-4 were destroyed during tunnelling process; hence, no data were recorded at the two points. According to the classical empirical equation describing the surface settlement trough (Peck 1969), the ground surface settlement due to tunnelling can be expressed as

$$S(x) = S_{\max} \exp\left(-\frac{x^2}{2i^2}\right) \quad (9)$$

$$S_{\max} = \frac{V_s}{i\sqrt{2\pi}} \quad (10)$$

$$V_L = \frac{V_s}{\pi R^2} \quad (11)$$

where $S(x)$ denotes the ground surface settlement at x (the horizontal offset from the tunnel centreline), S_{\max} is the maximum greenfield vertical surface displacement above the tunnel centreline, i is the transverse distance between the tunnel centreline and the inflection point of the settlement trough. V_s and R stand for the volume of the settlement trough (per metre length of tunnel) and the outer radius of the TBM, respectively. Based on existing research (Mair et al. 1993), a linear relationship with a

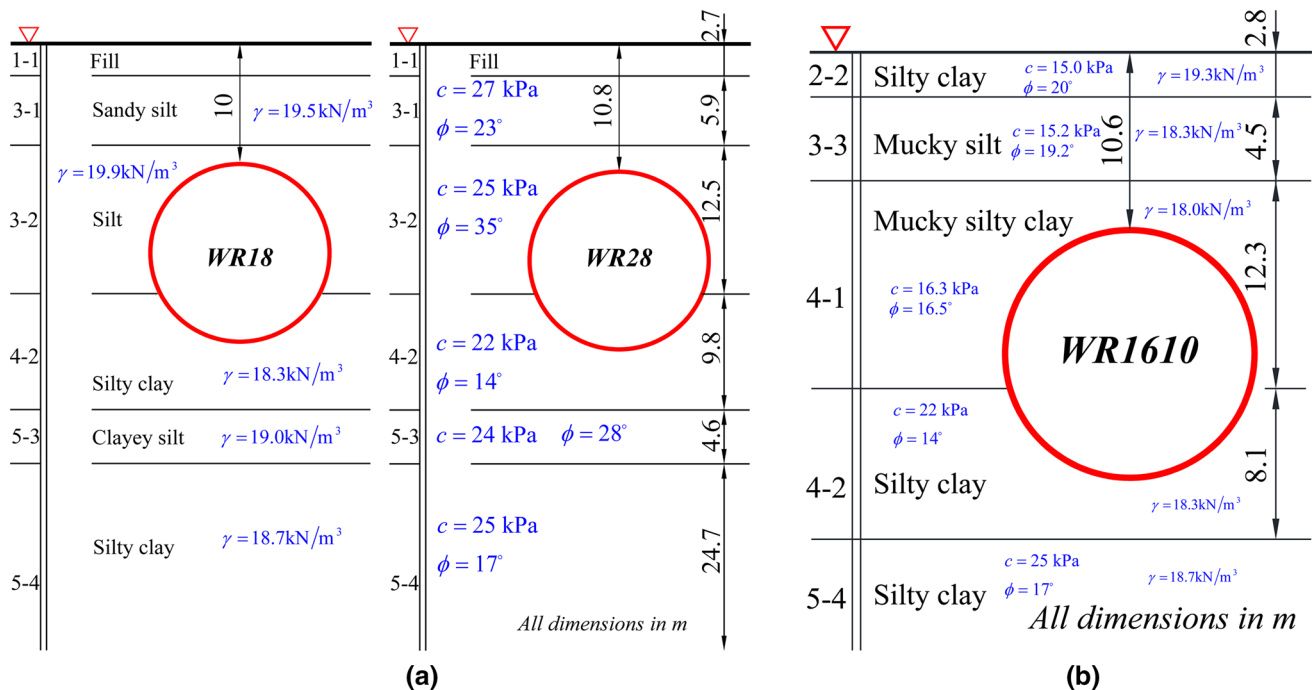


Fig. 8 Soil profiles of selected sections during WB tunnelling beneath the Qiantang River: **a** the south bank tunnelling (shield launching region); and **b** the north bank tunnelling (shield receiving region)

slope of $-0.5(i/z_0)^{-2}$ (z_0 is depth of tunnel centre level) exists between $\ln(S/S_{max})$ and $(x/z_0)^2$ if the surface settlement trough can be described as a Gaussian curve. As illustrated in Fig. 10 (only available data are presented), the calculated face ‘take’ V_L of the three sections are, respectively, 0.04, 0.08, and 0.05%, indicating slight tunnelling-induced impacts on ground surface settlement.

According to Eq. (2), V_L is associated with LF , ϵ_{50} , and C/D . Since the support media is slurry which is able to provide a linearly distributed pressure at the tunnel face, only FEA cases with hydrostatic support pressure are taken as references. Therefore, the critical stability ratios (N_c) are obtained by linear interpolation and linear extrapolation of the data presented in Table 3. Soil parameters (i.e. c and ϕ) employed in the interpolation and extrapolation are thickness-weighted mean values of the layers above the tunnel axis level. The weighted average approach is usually employed in homogenisation of the tunnel face, since it is simple to utilize in practice and is able to provide a big picture for the shear strengths of layered soils (Zizka and Thewes 2016). For WR18 and WR28, the averaged soil parameters are ($c = 26.0$ KPa, $\phi = 29.2^\circ$) and ($c = 25.9$ kPa, $\phi = 29.4^\circ$), respectively. The cover-to-diameter ratios of the two sections are 0.65 and 0.70, respectively. The support pressures (σ_t) are collected from sensors installed at the working face of the shield machine. ϵ_{50} of the soil at sections WR18 and WR28 is based on a series of triaxial tests carried out by Yang (2011). For soil at section WR1610, ϵ_{50} is obtained from another experimental study conducted by Li (2015). The undrained

shear strength s_u in Table 4 is obtained from unconsolidated undrained (UU) triaxial tests on soils at the tunnel centre level. As can be seen from Table 4, the predicted volume losses via Eq. (2) show good agreement with field observations. The monitored volume losses in the three sections WR18, WR28, and WR1610 are, respectively, 0.04, 0.08, and 0.05%, smaller than those based on the numerical results which are 0.06, 0.10, and 0.07%, respectively. The differences might be caused by the soil uniformity above the tunnel axis. It can be seen that although Eq. (2) is based on the assumption that soils considered are Tresca-like materials, i.e. pure cohesive soils, it can still be utilised for frictional materials under undrained condition. According to Eq. (2), V_L is significantly influenced by the inherent property (ϵ_{50}) of the soil at tunnel heading. The parameter ϵ_{50} should be carefully examined prior to utilisation. A better soil homogenisation approach should be employed instead of the thickness-weighted approach which is adopted in this study. Based on the field measurements, it can be concluded that tunnel face at the three sections was well supported without a collapse failure.

Face stability analysis for the URUP demonstration tunnel in China

URUP tunnelling method was initially developed in Japan (Hayashi et al. 2006) and has been employed in multiple tunnels (Nakamura and Hazama 2010). This tunnelling method is characterised by shield launching and receiving on the ground surface instead of within a working shaft for

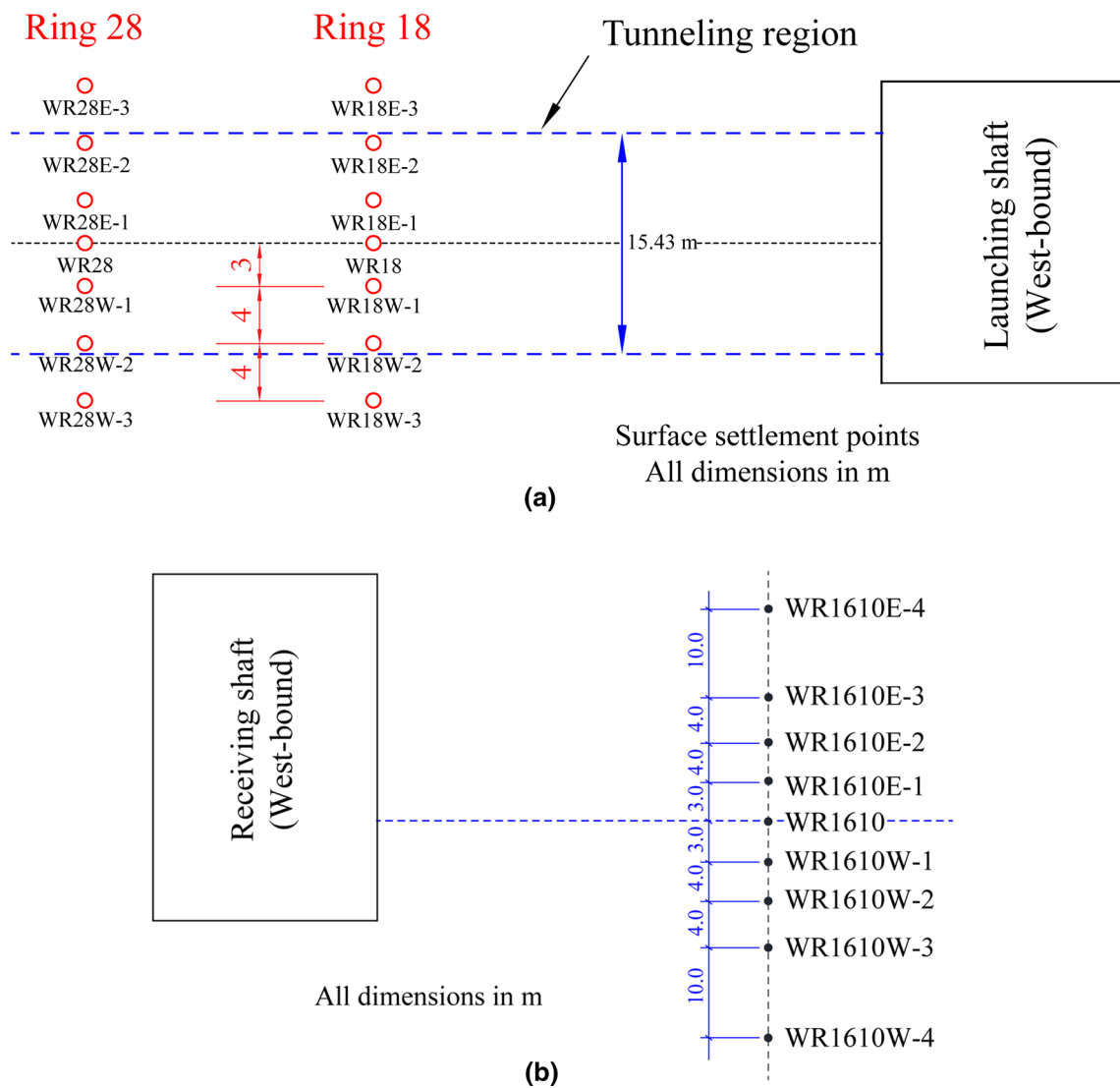


Fig. 9 Layout of field measurements for surface ground settlement: **a** at the south bank of WB route; **b** at the north bank of WB route

which large excavation is inevitable. Figure 11 illustrates a typical URUP tunnelling process. This method was put into application during construction of Metro Line S1 of Nanjing, the capital of Jiangsu Province in East China (Liu et al. 2017; Zhang et al. 2016).

Figure 12 shows information on ground strata and ring numbers of the EB URUP tunnel of Metro Line S1 of Nanjing. SSPs were arranged at section ER12. Special attention is paid to sections ER12, ER72, ER78, and ER85, corresponding to C/D of 0.72, 0.50, 0, and -0.30 . It should be pointed out that ground dewatering was employed for tunnelling under a cover-to-diameter ratio less than 0.5, for the sake of enhancing soil strength and reducing tunnelling-induced influence. Table 5 demonstrates comparison between volume loss obtained from Eq. 2 and that from surface settlement profile by field observation. ϵ_{50} and s_u are based on previous experimental research performed

by Li (2007). σ_t is acquired from field records of shield machine. N_c is calculated from the FEA results herein by linear interpolation and linear extrapolation. The predicted volume loss by the FEA is 0.07%, slightly smaller than that from field observation (0.08%), indicating a good applicability of Eq. (2) with the input of the critical stability ratio computed by FEA (i.e. $N_c = 5.8$). Different from section ER12 where UU condition is considered (underground water table was within 1 m below the ground surface), ground at the other three sections (ER72, ER78, and ER85) cannot be treated as UU condition after dewatering. Therefore, Eq. (2) is not applicable anymore. According to the FEA results of cases with $C/D = 0$ and -0.3 , tunnel face is able to maintain stability without support pressure when soils ahead of it are characterised by a cohesion greater than 20 kPa together with a friction angle larger than 10° . This agrees with the field observation for sections

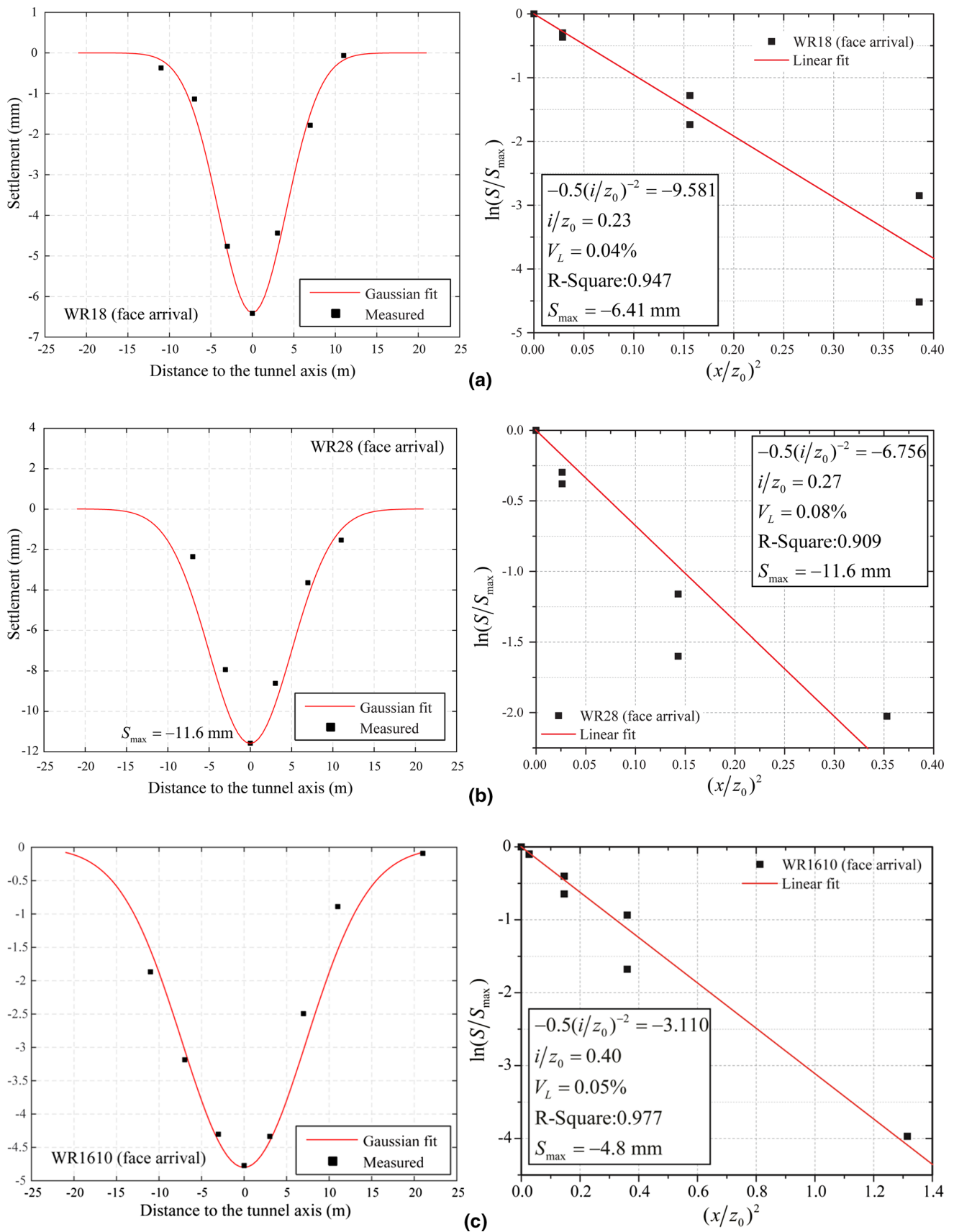


Fig. 10 Surface settlement trough and volume loss calculation of the selected monitoring sections: **a** section WR18; **b** section WR 28; and **c** WR 1610

Table 4 Comparison of V_L between numerical and theoretical predictions in the Qiantang River Tunnel

	C/D	N_c	N	σ_t (kPa)	LF	ϵ_{50}	s_u (kPa)	V_{L-n} (%)	V_{L-m} (%)
WR18	0.65	7.09	3.96	250	0.56	0.0006	25	0.06	0.04
WR28	0.70	7.27	3.76	255	0.52	0.0006	25	0.10	0.08
WR1610	0.69	7.36	5.38	227	0.73	0.0002	20	0.07	0.05

V_{L-n} , V_L based on N_c obtained from the FEA; V_{L-m} , V_L based on monitored surface settlement

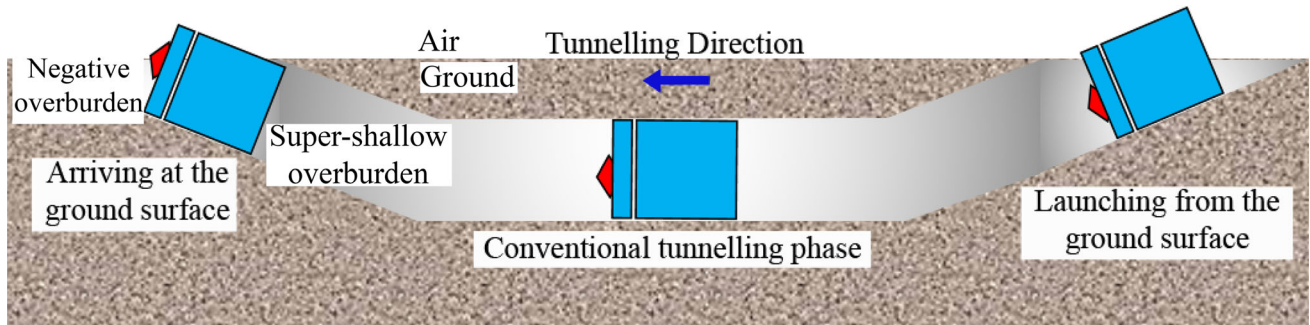


Fig. 11 Sketch illustrating the URUP tunnelling process Zhang et al. (2016)

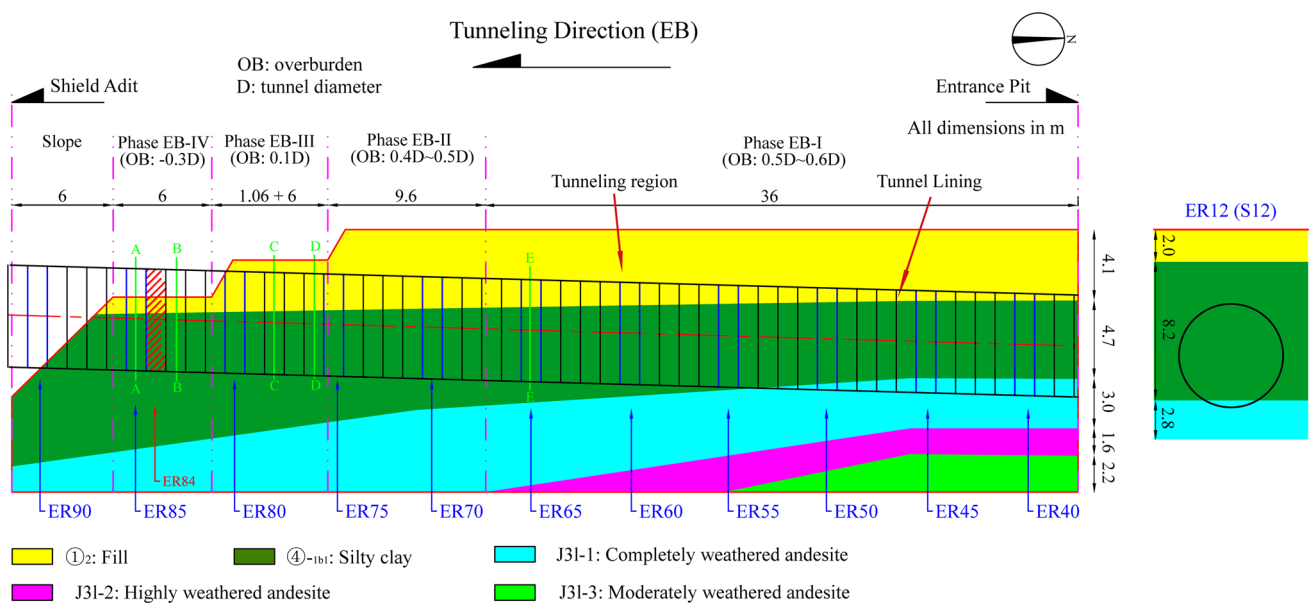


Fig. 12 Soil profile and monitoring sections during EB tunnelling

Table 5 Comparison of V_L between numerical prediction and field observation in the URUP demonstration tunnel

	C/D	N_c	N	σ_t (kPa)	LF	ϵ_{50}	s_u (kPa)	V_{L-n} (%)	V_{L-m} (%)
ER12	0.72	5.8	0.87	60	0.15	0.002	100	0.07	0.08

ER78 and ER85 in which $\sigma_t/\gamma D = 0$ as demonstrated in Table 6. The field record reveals that working chamber of the URUP shield machine was nearly empty during receiving on the ground surface (as shown in Fig. 13), implying that the tunnel face was unsupported at that time.

The self-stability is probable attributed to the ground dewatering as well as the inherent high shear strength of the soils ($s_u = 100$ kPa). The dewatering can improve the shear strength of the soil, making the frictional angle approaching the effective friction angle of the soil. For

Table 6 Critical support pressure during URUP tunnelling with $C/D = 0.5, 0,$ and -0.3

	C/D	σ_c (kPa)	σ_t (kPa)	$\sigma_c/\gamma D$	$\sigma_t/\gamma D$	c_c (kPa)	ϕ_c (°)
ER85	-0.30	0	0	0	0	70	18
ER78	0	0	0	0	0	70	18
ER72	0.50	5.8	60	0.02	2.46	70	18

σ_c and $\sigma_c/\gamma D$ are based on the FEA in this study; σ_t and $\sigma_t/\gamma D$ are obtained from field records; c_c and ϕ_c are cohesion and frictional angle obtained from CU (consolidated undrained) triaxial test



Fig. 13 Photograph of the URUP TBM during receiving on the ground surface

section ER72 where $C/D = 0.5$, a support pressure of 60 kPa was applied during TBM advance. This support pressure resulted in a $\sigma_t/\gamma D$ (i.e. 2.46) apparently greater than that at collapse (i.e. 0.02) in the FEA; hence, an upheaval of 1.8 mm above the tunnel centreline was observed during field measurement [for detailed information about the field measuring data, please refer to the previous research Liu et al. (2017)].

Conclusions

The paper presents a parametric numerical study on tunnel face stability, considering different cover-to-diameter ratio (C/D), different shear strength parameters (c and ϕ), and different distributions of support pressure. The support pressure was reduced stepwise in the FEA until simulation failure occurred. The reduced support pressure at the last step of simulation was adopted as the critical support pressure for collapse failure. Mohr–Coulomb criterion was employed to represent soil plasticity. By comparison between the results, respectively, obtained from small-strain FEA and finite-strain FEA, it can be concluded that small strain is inappropriate for FEA of failure process at tunnel face, owing to the lower (or rather more dangerous) predicted critical support pressure compared to the finite-strain FEA.

According to the FEA results, c and ϕ have different influences on critical support pressure at collapse. For the cases with $C/D > 0$ which are commonly seen in tunnelling activities, the critical support pressure ratio becomes more sensitive to ϕ than c with the increasing cover-to-diameter ratio. For the cases with $C/D = 0$, ϕ has little influence on the critical support pressure ratio when $\phi > 10^\circ$, while the critical support pressure ratio depends on both c and ϕ when $\phi < 10^\circ$. The critical support pressure ratio is not sensitive to support pressure distribution pattern when shear strength of tunnel-heading soil is relatively high, e.g. $c > 40$ kPa and $\phi > 40^\circ$. The FEA also revealed that cover-to-diameter ratio has limited influence on normalised critical support pressure ($\sigma_c/\gamma D$) in cohesionless soils when $C/D \leq 2.0$. Moreover, the normalised critical support pressure $\sigma_c/\gamma D$ increases consistently with C/D for soil with $\phi < 10^\circ$, probably attributed to the low level of friction angle which makes the soil deform significantly. Comparison to existing experimental data revealed that the FEA results in this study are reliable for investigating the critical support pressure in natural sandy soils. Critical stability ratio has a positive correlation with cover-to-diameter ratio under certain cohesion (except $c = 10$ kPa). As for cases with $c = 10$ kPa, critical stability ratios are evidently smaller than those with other three cohesions (20, 30, and 40 kPa) since local failure with a hemisphere mode occurs at tunnel heading.

A design chart has been developed for determining the critical stability ratio N_c based on numerical simulation results. Given that the soil strength parameters and depth-to-diameter ratio of the tunnel are known, the critical support pressure ratio N_c can be readily obtained from this design chart by interpolation and extrapolation. The volume loss can then be roughly estimated using the Klar and Klein’s formula. Two case studies are selected as references to validate the applicability of this methodology. Comparison between field measurement data and numerical simulation results reveals that the volume loss, predicted by Klar and Klein’s formula with the input of the critical stability ratio calculated by FEA, shows good agreement with field observation. It should be pointed that the natural properties of the soil are complex and usually not totally independent from each other, which means artificially determined parameters should be carefully

examined in constitutive modelling according to the reality. Thus, the design chart should be carefully examined in tunnelling practice and only used in rough evaluation for the volume loss during tunnelling.

Acknowledgements The research was conducted with funding provided by the National Science Foundation of China (Grant Nos. 41372276 & 51509186). The second author would like to acknowledge the support provided by Guangzhou University (Grant No. 2700050340). The first and second authors would like to acknowledge the support provided by Shanghai Tunnelling Engineering Co., Ltd.

References

- Anagnostou G (2012) The contribution of horizontal arching to tunnel face stability. *Geotechnik* 35:34–44
- Anagnostou G, Kovari K (1994) The face stability of slurry-shield-driven tunnels. *Tunn Undergr Space Technol* 9(2):165–174
- Anagnostou G, Kovari K (1996) Face stability conditions with earth-pressure-balanced shields. *Tunn Undergr Space Technol* 11:165–173
- Belter B, Heiermann W, Katzenbach R, Maidl B, Quick H, Wittke W (1999) NBS Köln-Rhein/Main-Neue Wege bei der Umsetzung von Verkehrsprojekten. *Bauingenieur* 74:1–7
- Broere W (2001) Tunnel face stability and new CPT applications. Ph.D. thesis, Delft University of Technology, The Netherlands
- Broms BB, Bennermark H (1967) Stability of clay at vertical opening. *J Soil Mech Found Div* 93(1):71–94
- Cairncross AM (1973) Deformations around model tunnels in stiff clay. Ph.D. thesis, University of Cambridge
- Casarin C, Mair R (1981) The assessment of tunnel stability in clay by model tests. In: Reséndiz D, Romo MP (eds) *Soft-ground tunnelling: failures and displacements*. A.A. Balkema, Rotterdam, pp 33–34
- Chambon P, Corte J-F (1994) Shallow tunnels in cohesionless soil: stability of tunnel face. *J Geotech Eng* 120(7):1148–1165
- Chen WF (1975) *Limit analysis and soil plasticity*. Elsevier, Amsterdam
- Chen RP, Tang LJ, Ling DS, Chen YM (2011) Face stability analysis of shallow shield tunnels in dry sandy ground using the discrete element method. *Comput Geotech* 38(2):187–195
- Chen RP, Li J, Kong LG, Lj Tang (2013) Experimental study on face instability of shield tunnel in sand. *Tunn Undergr Space Technol* 33:12–21
- Chen RP, Tang LJ, Yin XS, Chen YM, Bian XC (2015) An improved 3D wedge-prism model for the face stability analysis of the shield tunnel in cohesionless soils. *Acta Geotech* 10:683–692
- Coulomb C (1773) Sur une application des règles de maximis et minimis á quelques problèmes relatifs á l'architecture. *Mémoire Acad R Sci* 7:343–382
- Dassault Systèmes Simulia Corp (2014) *Abaqus user's manual*, version 6.14. Providence, R.I., USA
- Davis EH, Gunn MJ, Mair RJ, Seneviratne HN (1980) The stability of shallow tunnels and underground openings in cohesive material. *Geotechnique* 30(4):397–416
- Dimmock PS, Mair RJ (2007) Estimating volume loss for open-face tunnels in London Clay. *Proc Inst Civ Eng-Geotech* 160(1):13–22
- Drucker DC, Prager W (1952) Soil mechanics and plastic analysis or limit design. *Q Appl Math* 10:157–165
- Fan Z, Zhang Z (2013) Model test of excavation face stability of EPB shield in sandy cobble ground and adjacent building effect. *Yanshilixue Yu Gongcheng Xuebao/Chin J Rock Mech Eng* 32(12):2506–2512 (in Chinese)
- Harding H (1981) *Tunnelling history and my own involvement*. Golder Associates, Toronto
- Hayashi M, Miki K, Yokomizo F, Yoshida M, Izawa M (2006) The demonstration work of URUP method. In: *Proceedings of the 61st annual conference of Japan society of civil engineers*. Shiga Prefecture, pp 485–486
- Horn M (1961) Horizontal earth pressure on perpendicular tunnel face. In: *Hungarian national conference of the foundation engineer industry*, Budapest, pp 7–16
- Huang R (2008) *Overview of Shanghai Yangtze River tunnel project. Geotechnical Aspects of Underground Construction in Soft Ground*. CRC Press, Boca Raton
- Idinger G, Aklík P, Wu W, Borja RI (2011) Centrifuge model test on the face stability of shallow tunnel. *Acta Geotech* 6(2):105–117
- Jancsecz S, Steiner W (1994) Face support for a large mix-shield in heterogeneous ground conditions. *Tunnelling '94*. Springer, pp 531–550
- Kamata H, Mashimo H (2003) Centrifuge model test of tunnel face reinforcement by bolting. *Tunn Undergr Space Technol* 18:205–212
- Kanayasu S, Kubota I, Shikibu N (1995) Stability of face during shield tunneling—a survey of Japanese shield tunneling. *Undergr Construct Soft Ground* pp 337–343
- Karim ASMM (2007) *Three-dimensional discrete element modeling of tunneling in sand*. Ph.D. thesis, Canada: University of Alberta
- Kirsch A (2010) Experimental investigation of the face stability of shallow tunnels in sand. *Acta Geotech* 5(1):43–62
- Klar A, Klein B (2014) Energy-based volume loss prediction for tunnel face advancement in clays. *Geotechnique* 64(20):776–786
- Leca E, Dormieux L (1990) Upper and lower bound solutions for the face stability of shallow circular tunnels in frictional material. *Geotechnique* 40(4):581–606
- Leca E, Dormieux L (1992) Contribution à l'étude de la stabilité du front de taille d'un tunnel en milieu cohérent. *Rev Française Géotech* 61:5–16
- Lee IM, Nam SW, Ahn JH (2003) Effect of seepage forces on tunnel face stability. *Can Geotech J* 40(2):342–350
- Li S (2007) *Experiment and performance analysis of shear band for cohesive soil*. Ph.D. thesis, Nanjing University of Technology, Nanjing, China (in Chinese)
- Li Y (2008) *Stability analysis of large slurry shield-driven tunnel in soft clay*. Ph.D. thesis, Tongji University, Shanghai (in Chinese)
- Li Z (2015) *Deformation and stability investigation of underground excavations of subway transit system in soft clay*. Zhejiang University, Hangzhou (in Chinese)
- Li Y, Emeriault F, Kastner R, Zhang ZX (2009) Stability analysis of large slurry shield-driven tunnel in soft clay. *Tunn Undergr Space Technol* 24(4):472–481
- Liu C, Zhang ZX, Regueiro RA (2014) Pile and pile group response to tunnelling using a large diameter slurry shield—case study in Shanghai. *Comput Geotech* 59:21–43
- Liu C, Zhang ZX, Kwok CY, Jiang HQ, Teng L (2017) Ground responses to tunneling in soft soil using the URUP method. *J Geotech Geoenviron Eng* 143(7):04017023
- Lu X, Wang H, Huang M (2014) Upper bound solution for the face stability of shield tunnel below the water table. *Math Probl Eng* 2014:1–11
- Macklin SR (1999) The prediction of volume loss due to tunnelling in overconsolidated clay based on heading geometry and stability number. *Ground Eng* 32(4):30–33
- Mair RJ (1979) *Centrifugal modelling of tunnel construction in soft clay*. Ph.D. thesis, Cambridge University

- Mair R (1993) Unwin memorial lecture 1992: developments in geotechnical engineering research: application to tunnels and deep excavations. *Proc Inst Civ Eng Civ Eng* 97(1):27–41
- Mair R, Taylor R (1997) Bored tunnelling in the urban environment. In: *The 14th international conference on soil mechanics and foundation engineering*, Rotterdam, pp 2353–2385
- Mair R, Gunn M, O'Reilly M (1981) Ground movements around shallow tunnels in soft clay. In: *The 10th international conference on soil mechanics and foundation engineering: international society for soil mechanics and foundation engineering*, pp 323–328
- Mair RJ, Taylor RN, Bracegirdle A (1993) Subsurface settlement profiles above tunnels in clays. *Geotechnique* 43(2):315–320
- Maynar MJM, Rodriguez L (2005) Discrete numerical model for analysis of earth pressure balance tunnel excavation. *J Geotech Geoenviron* 131(10):1234–1242
- Mollon G, Dias D, Soubra AH (2010) Face stability analysis of circular tunnels driven by a pressurized shield. *J Geotech Geoenviron* 136(1):215–229
- Mollon G, Dias D, Soubra AH (2013) Continuous velocity fields for collapse and blowout of a pressurized tunnel face in purely cohesive soil. *Int J Numer Anal Methods* 37(13):2061–2083
- Nakamura T, Hazama H (2010) URUP (Ultra Rapid under Pass) method the first implementation in a public project. In: *The 5th civil engineering conference in the asian region and Australasian structural engineering conference 2010*, Engineers Australia, Sydney, pp 1175–1180
- Peck RB (1969) Deep excavations and tunneling in soft ground. In: *The 7th international conference on soil mechanics and foundation engineering: Sociedad Mexicana de Mecánica*, pp 225–290
- Schofield AN (1980) *Cambridge geotechnical centrifuge operations*. *Geotechnique* 30(3):227–268
- Soubra AH (2000) Three-dimensional face stability analysis of shallow circular tunnels. In: *ISRM international symposium*. International Society for Rock Mechanics, Melbourne, Australia
- Soubra AH (2002) Kinematical approach to the face stability analysis of shallow circular tunnels. In: *8th international symposium on plasticity*. British Columbia, Canada
- Tang X-W, Liu W, Albers B, Savidis S (2014) Upper bound analysis of tunnel face stability in layered soils. *Acta Geotech* 9(4):661–671
- Vermeer PA, Ruse N, Marcher T (2002) Tunnel heading stability in drained ground. *Felsbau* 20(6):8–18
- Wong KS, Ng CWW, Chen YM, Bian XC (2012) Centrifuge and numerical investigation of passive failure of tunnel face in sand. *Tunn Undergr Space Technol* 28:297–303
- Yang Y (2011) Experimental study on engineering properties of Qiantang alluvial silts. Zhejiang University, Hangzhou (**in Chinese**)
- Zhang ZX, Hu XY, Scott KD (2011) A discrete numerical approach for modeling face stability in slurry shield tunnelling in soft soils. *Comput Geotech* 38(1):94–104
- Zhang C, Han K, Zhang D (2015) Face stability analysis of shallow circular tunnels in cohesive–frictional soils. *Tunn Undergr Space Technol* 50:345–357
- Zhang ZX, Liu C, Huang X, Kwok CY, Teng L (2016) Three-dimensional finite-element analysis on ground responses during twin-tunnel construction using the URUP method. *Tunn Undergr Space Technol* 58:133–146
- Zizka Z, Thewes M (2016) Recommendations for face support pressure calculations for shield tunnelling in soft ground. German Tunnelling Committee (ITA-AITES), Cologne, Germany